

Reverse time migration in tilted transversely isotropic (TTI) media

Robin P. Fletcher¹, Xiang Du¹, and Paul J. Fowler²

ABSTRACT

Reverse time migration (RTM) exhibits great advantages over other imaging methods because it is based on computing numerical solutions to a two-way wave equation. It does not suffer from dip limitation like one-way downward continuation techniques do, thus enabling overturned reflections to be imaged. As well as correctly handling multipathing, RTM has the potential to image internal multiples when the boundaries responsible for generating the multiples are present in the model. In isotropic media, one can use a scalar acoustic wave equation for RTM of pressure data. In anisotropic media, P- and SV-waves are coupled together so, formally, elastic wave equations must be used for RTM. A new wave equation for P-waves is proposed in tilted transversely isotropic (TTI) media that can be solved as part of an acoustic anisotropic RTM algorithm, using standard explicit finite differencing. If the shear velocity along the axis of symmetry is set to zero, stable numerical solutions can be computed for media with a vertical axis of symmetry and ε not less than δ . In TTI media with rapid variations in the direction of the axis of symmetry, setting the shear velocity along the axis of symmetry to zero can cause numerical solutions to become unstable. A solution to this problem is proposed that involves using a small amount of nonzero shear velocity. The amount of shear velocity added is chosen to remove triplications from the SV wavefront and to minimize the anisotropic term of the SV reflection coefficient. We show modeling and high-quality RTM results in complex TTI media using this equation.

INTRODUCTION

Reverse time migration (RTM) propagates the source wavefield forward and the recorded wavefield backward in time using a two-

way wave equation (Baysal et al., 1983; McMechan, 1983; Whitmore, 1983). It correctly handles both multi-arrivals and the phase changes caused by caustics. It has virtually no dip limitation, which enables imaging of overturned reflections, and can be used to image some forms of multiple (e.g., prismatic) energy. In isotropic media, we can solve efficiently the scalar acoustic wave equation instead of the more expensive elastic wave equation to perform acoustic RTM of pressure data.

Seismic anisotropy is observed in many exploration areas. Conventional isotropic RTM for seismic imaging is insufficient in these areas. Even when multicomponent data are available, one of the complexities that impedes anisotropic elastic RTM is the difficulty of separating anisotropic wavefields into different wave modes for imaging (Yan and Sava, 2008). Rather than solving the complicated anisotropic elastic wave equation, many researchers have derived simpler two-way wave equations that can be solved efficiently to perform acoustic anisotropic RTM of pressure data.

Alkhalifah (1998) introduces a pseudo-acoustic approximation for transversely isotropic (TI) media by setting the shear velocity along the axis of symmetry to zero. Although this dispersion relation for a scalar wavefield has kinematics close to those of the P arrivals in the real elastic vector wavefield, it allows spurious SV events (Grechka et al., 2004). Many researchers have derived and implemented two-way wave equations for vertical transversely isotropic (VTI) media starting from Alkhalifah's dispersion relation (Alkhalifah, 2000; Klie and Toro, 2001; Zhou et al., 2006a; Hestholm, 2007; Du et al., 2008). Alternatively, starting with Hooke's law and the equations of motion, vertical shear velocity can be set to zero to derive a pseudo-acoustic VTI wave equation (Duvencack et al., 2008). Tilting the symmetry axis relative to the coordinates does not add any new physics but rather more algebraic complexity. Several pseudo-acoustic tilted transversely isotropic (TTI) wave equations derived by setting the shear velocity along the axis of symmetry to zero have already been proposed (Zhou et al., 2006b; Fletcher et al., 2008; Zhang and Zhang, 2008).

Manuscript received by the Editor 19 December 2008; revised manuscript received 13 February 2009; published online 15 December 2009.

¹WesternGeco, Schlumberger House, Gatwick Airport, West Sussex, England. E-mails: rfletcher1@gatwick.westerngeco.slb.com; xdu@crawley.oilfield.slb.com.

²WesternGeco, Denver, Colorado, U.S.A. E-mail: pfowler1@slb.com.

© 2009 Society of Exploration Geophysicists. All rights reserved.

In the next section, we focus on a new pseudo-acoustic TTI wave equation derived using the ‘‘asymptotically’’ exact P-SV dispersion relation and parameterized using the anisotropic parameters ε and δ , defined by [Thomsen \(1986\)](#). For media with a constant vertical axis of symmetry and ε greater than or equal to δ , it is straightforward to implement modeling and migration with the vertical shear velocity set to zero. However, for modeling and migration in heterogeneous TTI media, a variably oriented axis of symmetry can cause instabilities with numerical implementations. Making the shear velocity finite along the axis of symmetry can remove propagation instabilities arising from tilt axis variation and from places where ε is less than δ . We will detail how to choose the shear velocity to stabilize propagation in heterogeneous TTI media while minimizing SV-waves considered as artifacts for acoustic modeling and migration. In the numerical experiments section, we demonstrate forward modeling and migration (RTM) using this new wave equation.

METHOD

Solving the Christoffel equations for homogeneous TTI media gives three distinct wave modes: P, SV, and SH ([Tsvankin, 2001](#)). The SH mode decouples, leaving a fourth-order dispersion equation describing the propagation of the coupled P and SV modes. Correctly, this dispersion relation describes wave speeds for the distinguished vector polarizations corresponding to the P- or SV-waves. However, we can also treat it as defining the propagation of a scalar, pseudo-acoustic wavefield. The P-SV TTI dispersion relation derived from the Christoffel equations can be written as

$$\begin{aligned} \omega^4 = & [(v_{px}^2 + v_{sz}^2)(\hat{k}_x^2 + \hat{k}_y^2) + (v_{pz}^2 + v_{sz}^2)\hat{k}_z^2]\omega^2 - v_{px}^2 v_{sz}^2 (\hat{k}_x^2 \\ & + \hat{k}_y^2)^2 - v_{pz}^2 v_{sz}^2 \hat{k}_z^4 + [v_{pz}^2(v_{pn}^2 - v_{px}^2) - v_{sz}^2(v_{pn}^2 + v_{pz}^2)] \\ & \times (\hat{k}_x^2 + \hat{k}_y^2)\hat{k}_z^2, \end{aligned} \quad (1)$$

where the hats over the wavenumbers (\hat{k}_x , \hat{k}_y , and \hat{k}_z) indicate that they are evaluated in a rotated coordinate system aligned with the symmetry axis. Here, ω is the angular frequency; v_{pz} is the P-wave velocity in the direction normal to the symmetry plane; $v_{pn} = v_{pz}\sqrt{1 + 2\delta}$ is the P-wave normal moveout (NMO) velocity — again, relative to the normal to the symmetry plane; $v_{px} = v_{pz}\sqrt{1 + 2\varepsilon}$ is the P-wave velocity in the symmetry plane; v_{sz} is the SV velocity normal to the symmetry plane; and ε and δ are anisotropic parameters defined by [Thomsen \(1986\)](#).

The corresponding fourth-order partial differential equation (PDE) in time, following immediately from equation 1, is cumbersome to solve. Mixed spatial derivatives exist that require more computation than derivatives in a single spatial variable because differencing operators become 2D or 3D convolutions rather than 1D. For this reason, we often seek to find equivalent coupled lower-order systems.

We have analyzed the space of possible coupled second-order in-time PDEs that can be derived from the P-SV dispersion relation in equation 1 ([Fowler et al., 2008](#)). Of the space of possible solutions, the most efficient to implement is the family of coupled second-order PDEs parameterized with a nonzero scalar α ,

$$\begin{aligned} \frac{\partial^2 p}{\partial t^2} &= v_{px}^2 H_2 p + \alpha v_{pz}^2 H_1 q + v_{sz}^2 H_1 (p - \alpha q) \\ \frac{\partial^2 q}{\partial t^2} &= \frac{v_{pn}^2}{\alpha} H_2 p + v_{pz}^2 H_1 q - v_{sz}^2 H_2 \left(\frac{1}{\alpha} p - q \right), \end{aligned} \quad (2)$$

where the differential operators H_1 and H_2 are given by

$$\begin{aligned} H_1 &= \sin^2 \theta \cos^2 \phi \frac{\partial^2}{\partial x^2} + \sin^2 \theta \sin^2 \phi \frac{\partial^2}{\partial y^2} + \cos^2 \theta \frac{\partial^2}{\partial z^2} \\ &+ \sin^2 \theta \sin 2\phi \frac{\partial^2}{\partial x \partial y} + \sin 2\theta \sin \phi \frac{\partial^2}{\partial y \partial z} \\ &+ \sin 2\theta \cos \phi \frac{\partial^2}{\partial x \partial z}, \\ H_2 &= \frac{\partial^2}{\partial x^2} + \frac{\partial^2}{\partial y^2} + \frac{\partial^2}{\partial z^2} - H_1, \end{aligned} \quad (3)$$

where θ is the dip measured to the vertical and ϕ the azimuth of the axis of symmetry. Note that for VTI, the differential operator H_1 acts only in the vertical direction whereas H_2 acts only in the horizontal direction; neither operator contains any mixed-space derivatives. In isotropic media, the two second-order PDEs in equation 2 are the same and wavefield p is equal to wavefield q . The derivation of this family of wave equations can be found in Appendix A.

Equation 2 could be solved with a pseudospectral method, carrying out the space derivative calculation in the wavenumber domain and time stepping by explicit finite differences. However, because pseudospectral methods require repeated Fourier transforms, it is challenging to parallelize computation for propagation in large models while avoiding wraparound artifacts. For these reasons, we solve equation 2 in the space-time domain using high-order finite differencing. We handle large models with domain decomposition with multiple compute nodes propagating separate domains of the model and periodically communicating their boundary information.

Although both the wavefields p and q are solutions to the fourth-order PDE corresponding to equation 1, we treat wavefield p as pressure and q as an auxiliary wavefield. Different choices of the parameter α result in different dynamic responses of the modelled wavefield. We implement equation 2 with a choice of $\alpha = 1$.

Evaluation of the constraint on the stiffness coefficients of TTI media (equation 1.51 in [Tsvankin, 2001](#)) gives the following stability condition:

$$\varepsilon - f^2 - f\delta + f + (1 - f)\sqrt{f(f + 2\delta)} \geq 0, \quad (4)$$

where

$$f = 1 - \frac{v_{sz}^2}{v_{pz}^2}. \quad (5)$$

This stability criterion reduces to just $\varepsilon - \delta \geq 0$ when one sets $v_{sz} = 0$.

Setting v_{sz} to zero

Starting from wave equation 2 and following Alkhalifah's example of setting the shear velocity along the symmetry axis to zero gives a pseudo-acoustic wave equation that can be solved more efficiently. When $\alpha = 1$, equation 2 reduces in VTI media to the wave equation proposed by Du et al. (2008). When the symmetry axis is nonvertical it reduces to the wave equation proposed by Fletcher et al. (2008) and Zhang and Zhang (2008). When $\alpha = v_{pn}/v_{pz}$, equation 2 reduces in VTI media to the wave equation proposed by Duveneck et al. (2008). In this case, Duveneck et al. (2008) are able to interpret physically the p wavefield as the horizontal stress component and the q wavefield as the vertical stress component.

NUMERICAL EXAMPLES

In all of the following 2D numerical examples, wave propagation is simulated using high-order finite differencing to solve equation 2. We used a finite-difference scheme that is second-order in time and eighth-order in space. The computational grid is chosen to avoid spatial dispersion and the propagation time step dt is chosen to satisfy the stability condition

$$dt \leq \frac{\mu \min\{dx, dz\}}{v_{px}}, \quad (6)$$

where μ is a stability constant, dx and dz are the grid cell sizes, and v_{px} is the fastest anisotropic velocity. A variable grid is used in the depth direction. Further standard optimizations can be applied easily.

Figures 1 and 2 show time snapshots of wave propagation in a 2D homogeneous anisotropic media ($v_{pz} = 3000$ m/s, $v_{sz} = 0$, $\varepsilon = 0.24$, and $\delta = 0.1$). Figure 1 corresponds to a vertical axis of symmetry and Figure 2 to an axis of symmetry tilting at 45° . The approximately

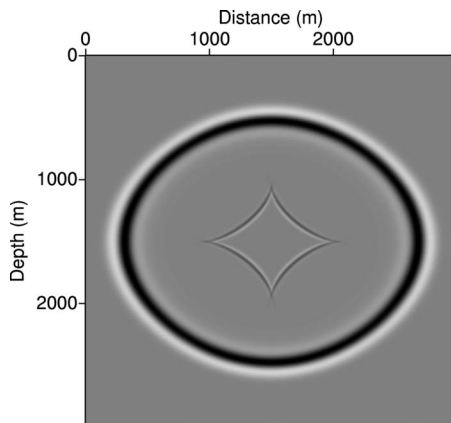


Figure 1. Wavefield snapshot in a homogeneous VTI medium: $v_{pz} = 3000$ m/s; $v_{sz} = 0$; $\varepsilon = 0.24$; and $\delta = 0.1$.

ellipsoidal compressional P wavefront and a diamond shape of the SV wavefront can be seen clearly. This SV-wave is a well-known problem, which for the purposes of P-wave modeling is considered as an artifact. It is generated only in anelliptic media ($\varepsilon \neq \delta$) and can be muted out from point-source modelling (Duveneck et al., 2008).

For RTM from marine acquisitions, sources and receivers are placed in an isotropic water layer. In this case, the source-generated SV artifact will not exist either for the forward-propagated source wavefield or the back-propagated receiver wavefield. However, SV artifacts can still arise from subsequent mode conversions from contrasts in the parameter model elsewhere. Figure 3 shows an impulse response for prestack RTM based on equation 2 in the same homogeneous anisotropic medium with a 45° tilting symmetry axis. In these examples, wave propagation is stable with a constant tilt axis.

We have found explicit centered finite-difference solutions to equation 2 when $v_{sz} = 0$ can be unstable in some media with varying azimuth and dip angle. The instabilities usually start at locations in the azimuth and dip models where sharp contrasts exist. Zhang and Zhang (2008) also note similar instabilities when using centered pseudospectral methods. These instabilities appear to arise from the interaction of the SV-wave artifact with rapid variations in the tilt axis. Smoothing the model can stabilize wave propagation but also can alter its kinematics significantly.

Our experiments indicate that adding finite v_{sz} terms provides an alternative and more accurate method to stabilize wave propagation. The question remains is what v_{sz} values to use. The following analysis details our approach to stabilizing propagation by using a reasonable finite v_{sz} in equation 2. Our approach also removes triplications from the SV wavefront and minimizes the anisotropic SV reflection coefficient.

Stabilizing propagation using a finite v_{sz}

The parameter

$$\sigma = \frac{v_{pz}^2}{v_{sz}^2} (\varepsilon - \delta) \quad (7)$$

largely determines the kinematic signatures of SV-waves in TTI media (Tsvankin, 2001). Figure 4 displays the kinematics of P and SV wavefronts in a strongly anisotropic homogeneous VTI medium

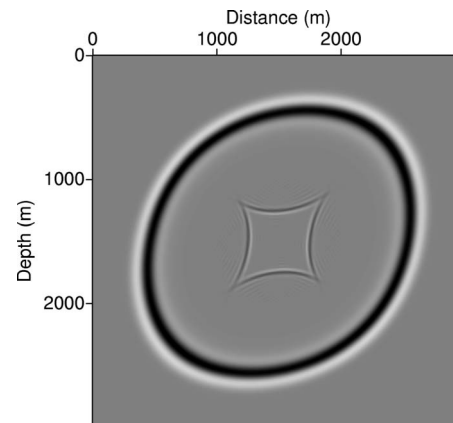


Figure 2. Wavefield snapshot in a homogeneous TTI medium: $v_{pz} = 3000$ m/s; $v_{sz} = 0$; $\varepsilon = 0.24$; $\delta = 0.1$; and $\theta = 45^\circ$.

($v_{pz} = 3000$ m/s, $\epsilon = 0.24$, $\delta = 0.1$) for various values of σ (and, hence, v_{sz}). As documented by Tsvankin (2001), triplications in the SV wavefront are removed for values of σ less than approximately

0.8. Our experiments indicate that choosing v_{sz} large enough (and, hence, σ small enough) to remove SV wavefront triplications gives stable wave propagation even with highly variable tilt-axis orientation.

The reflection coefficient of SV-waves at a small-contrast interface between two weakly anisotropic TI media can be expressed as the sum of the corresponding coefficient in isotropic media $R_{isor}(\theta)$ and the anisotropic term:

$$R_{aniso,SV}(\theta) \approx \frac{1}{2}(\sigma_1 - \sigma_2)\sin^2 \theta, \quad (8)$$

where σ_1 and σ_2 are the parameter values defined in equation 7 above and below the reflector, respectively (Tsvankin, 2001). Clearly, if we choose v_{sz} to ensure a constant value of σ over the whole

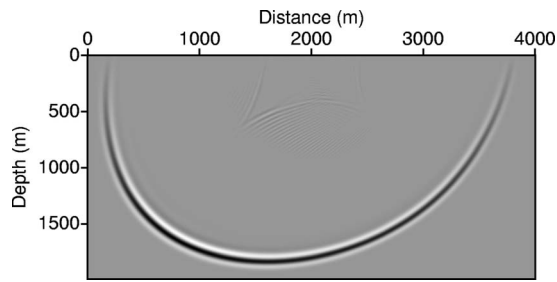


Figure 3. Impulse response from prestack RTM in a homogeneous TTI medium: $v_{pz} = 3000$ m/s; $v_{sz} = 0$; $\epsilon = 0.24$; $\delta = 0.1$; and $\theta = 45^\circ$.

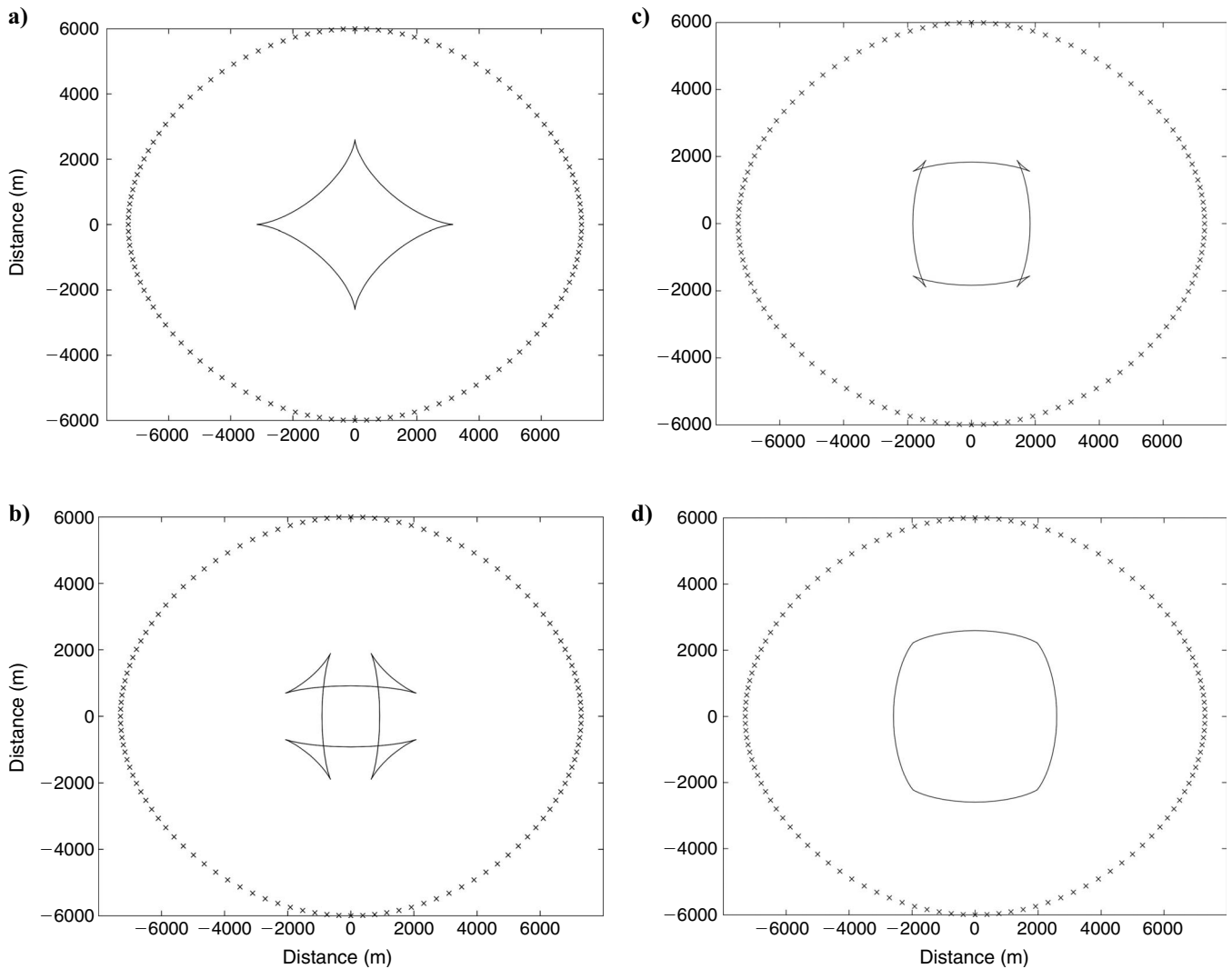


Figure 4. Kinematics of a P-wave (crosses) and a SV-wave (solid line) in a homogeneous VTI medium: $v_{pz} = 3000$ m/s; $\epsilon = 0.24$; and $\delta = 0.1$. The parameter $\sigma = \frac{v_{pz}^2}{v_{sz}^2}(\epsilon - \delta)$ controls triplications in the SV wavefront: (a) $\sigma = \infty$; (b) $\sigma = 6.0$; (c) $\sigma = 1.5$; and (d) $\sigma = 0.75$.

heterogeneous model, then this anisotropic term for the SV reflection coefficient will be zero everywhere. Taking this approach in isotropic and elliptically anisotropic media we ensure that v_{sz} is set to zero.

To demonstrate our approach of stabilizing propagation using a finite shear velocity along the axis of symmetry, we use the BP 2D TTI model. Figure 5 displays a small region of this model. There is complicated heterogeneity in all four parameters, including the dip angle for the axis of symmetry. Figure 6b displays a wavefield snapshot from a modeling experiment (without absorbing boundary conditions) in a small region of this model. Figure 6a displays the dip of the axis of symmetry parameter for the same region. The modeling performed here used equation 2 and set $v_{sz} = 0$. Clearly, the wave propagation is unstable when a high contrast exists in the dip field. Figure 6c displays the same time wavefront snapshot as in Figure 6b but set $v_{sz} = v_{pz}/2$ everywhere when using equation 2. The wave propagation is now stable. However, additional energy (highlighted in Figure 6c) is now present. This energy is caused by reflections of

the SV artifact. Figure 6d again displays the same time wavefront snapshot generated by setting v_{sz} to ensure $\sigma = 0.75$ everywhere. The wave propagation is again stable but without the unwanted SV reflections.

We implement this approach of stabilizing propagation using a finite shear velocity along the axis of symmetry within prestack TTI RTM and apply it on two data sets. First, we use the 2D overthrust model displayed in Figure 7. We migrate pressure data generated by Amoco using an elastic finite-difference modeling technique (Fei et al., 1998). Figure 8 displays the resulting RTM image. Reflectors are imaged in the correct position. Second, we apply TTI RTM to the 2D BP TTI data set corresponding to the model displayed in Figure 5. This is a high-quality data set generated by elastic finite-difference modeling with shot spacing of 50 m, receiver spacing of 12.5 m, and 10,025 m maximum offset. Figure 10 displays the resulting RTM image. For comparison, an equivalent TTI Kirchhoff depth-migration image is displayed in Figure 9. The RTM image shows better imaging of reflectors truncating up against the two salt bodies.

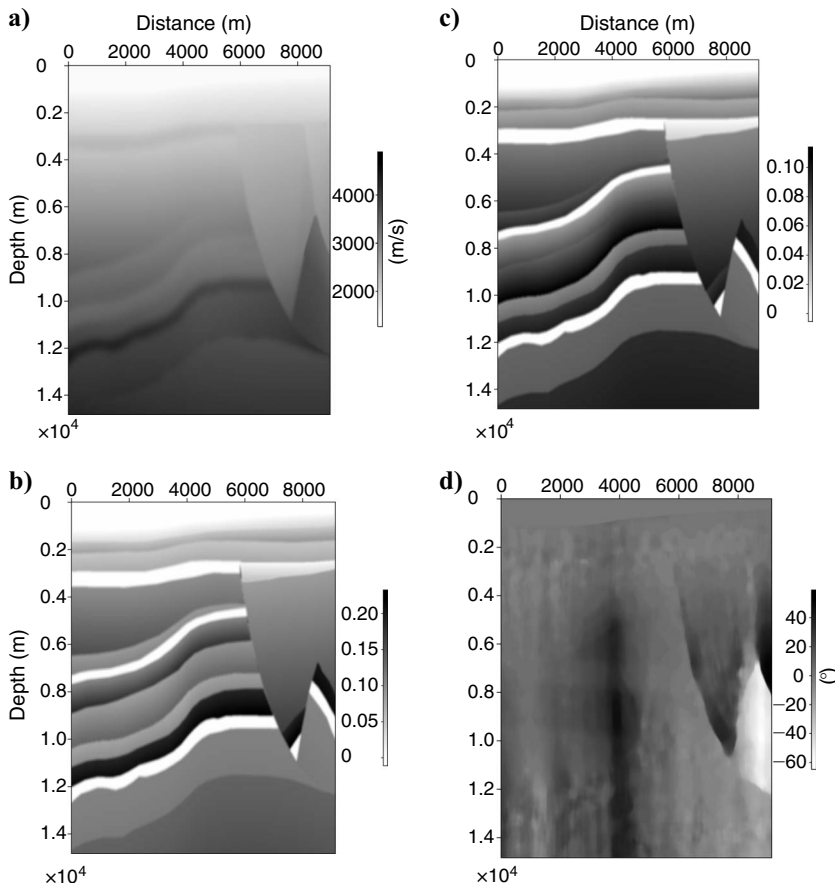


Figure 5. Partial region of the 2D BP TTI model: (a) v_{pz} ; (b) ϵ ; (c) δ ; and (d) θ .

Figure 6. Wavefield snapshots in the 2D BP TTI model: (a) model dip parameter θ ; (b) wavefield snapshot setting $v_{sz} = 0$. The wave propagation is unstable when a high contrast is present in the dip field; (c) wavefield snapshot setting $v_{sz} = v_{pz}/2$. The propagation is stable but additional reflections are visible; (d) wavefield snapshot setting $\sigma = 0.75$. Note that there are no absorbing boundary conditions used in this experiment.

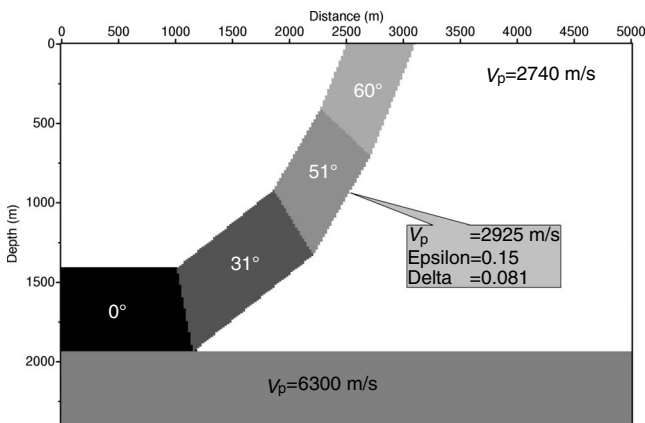
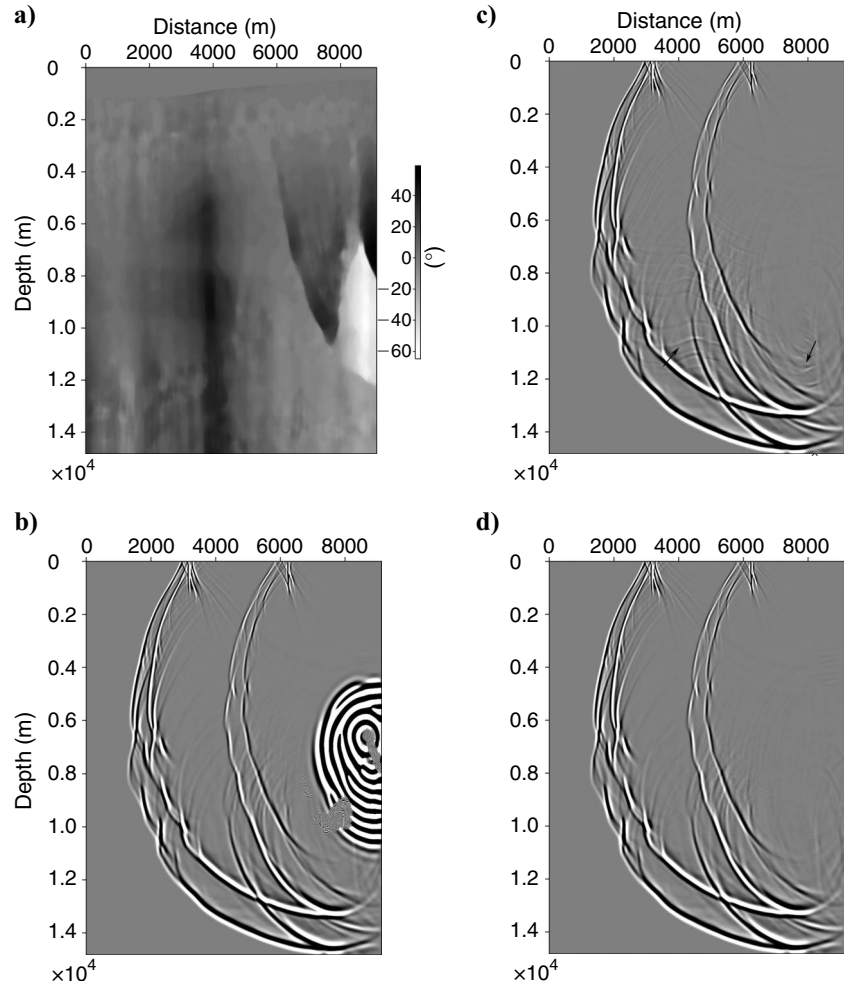


Figure 7. Two-dimensional TTI overthrust model.

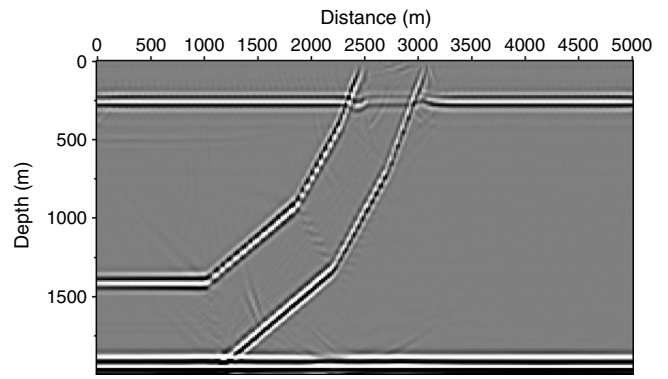


Figure 8. Prestack TTI RTM image of the 2D TTI overthrust model.

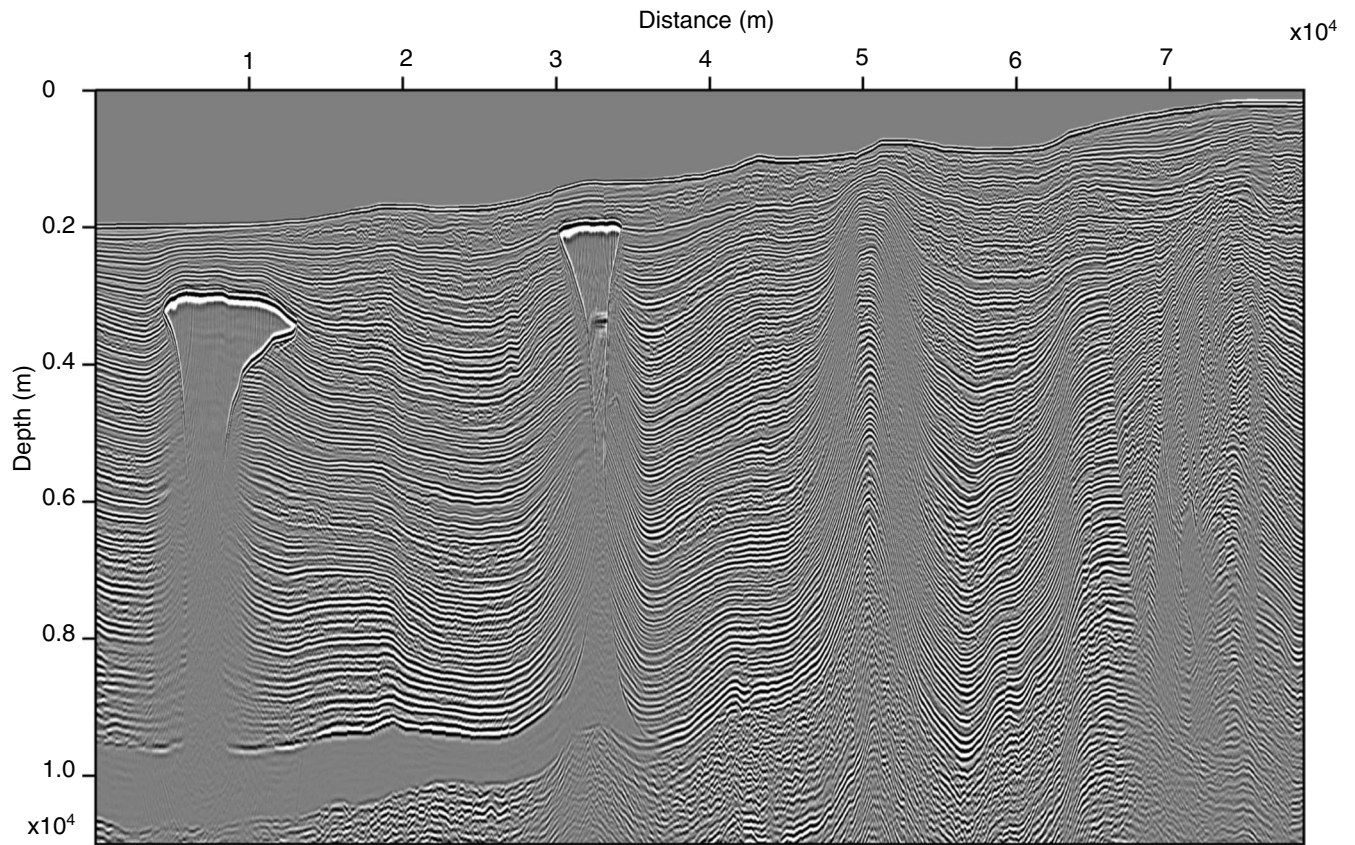


Figure 9. Prestack TTI Kirchhoff depth-migration image of the 2D BP TTI model.

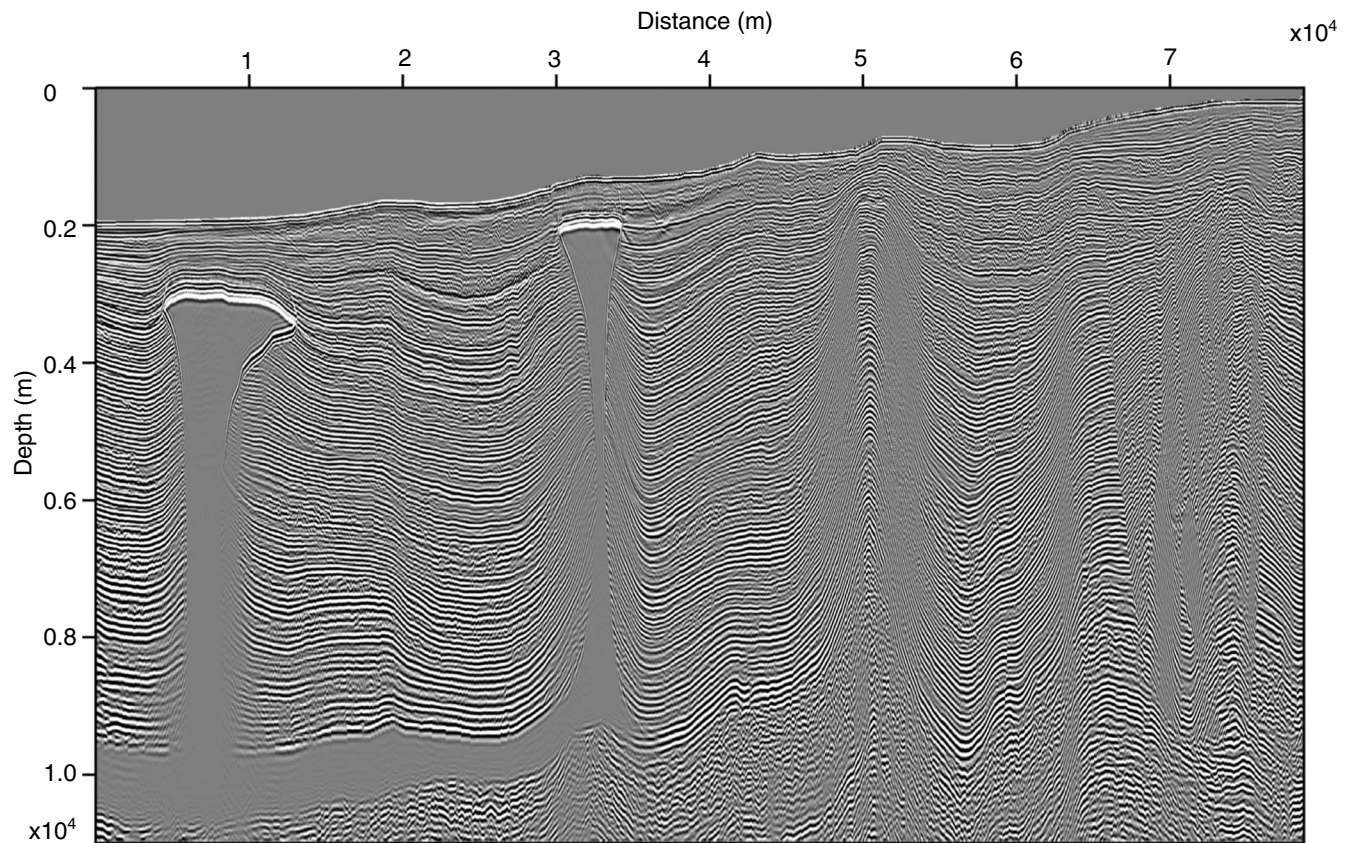


Figure 10. Prestack TTI RTM image of the 2D BP TTI model.

CONCLUSION

Prestack RTM is a powerful tool to image complex structures. We propose a new pseudo-acoustic wave equation for TTI media that can be solved as part of an acoustic anisotropic RTM algorithm using standard explicit finite differencing. Forcing the shear velocity along the axis of symmetry in this equation to zero gives a simpler wave equation. This reduced equation is more efficient to solve and is stable in VTI media where $\varepsilon - \delta \geq 0$. However, we observe that explicit finite-difference solutions of this simpler wave equation can become unstable in TI media, which have rapid variations in the orientation of the axis of symmetry. We propose a solution to this problem using a small finite shear velocity along the axis of symmetry, chosen to remove triplications from the SV wavefront and minimize the anisotropic term of the SV reflection coefficient. We show modeling and RTM results in complex 2D TTI media.

The proposed solution works equally well in complex 3D TTI media. A straightforward 3D TTI implementation using explicit finite differencing will involve approximately six times the amount of computation as a VTI solution. However, in model regions where the tilt axis is vertical or varies slowly, the shear velocity can be set to zero and not all computations of the wavefield derivatives are required. Using such optimizations can reduce costs significantly.

For the purposes of P-wave migration, the SV-waves that still can be generated at high contrasts in model parameters with the proposed approach are considered as an artifact. In our migration experiments, we have not observed any contamination from such energy in the stacked image. Investigation into whether this energy is significant on angle gathers produced from RTM is a topic for ongoing research.

ACKNOWLEDGMENTS

The authors would like to thank BP Amoco for making the TTI overthrust synthetic data set available and BP for making the 2007 2D TTI velocity benchmark data set and model available. We would also like to thank Yu Zhang, Hongbo Zhou, and one anonymous reviewer for their valuable comments and suggestions. Finally, we thank the management of WesternGeco for permission to publish these results.

APPENDIX A

DERIVATION OF THE PSEUDO-ACOUSTIC TTI WAVE EQUATION

If we let θ and ϕ be the rotation angles (θ is the dip angle measured to vertical, ϕ is the azimuth), then we have for the rotated wavenumbers:

$$\begin{aligned}\hat{k}_x &= k_x \cos \theta \cos \phi + k_y \cos \theta \sin \phi - k_z \sin \theta \\ \hat{k}_y &= -k_x \sin \phi + k_y \cos \phi \\ \hat{k}_z &= k_x \sin \theta \cos \phi + k_y \sin \theta \sin \phi + k_z \cos \theta.\end{aligned}\tag{A-1}$$

The dispersion relation in equation 1 then can be rewritten as

$$\omega^4 = ((v_{px}^2 + v_{sz}^2)f_2 + (v_{pz}^2 + v_{sz}^2)f_1)\omega^2 - v_{px}^2 v_{sz}^2 f_2 \cdot f_2$$

$$\begin{aligned}& - v_{pz}^2 v_{sz}^2 f_1 \cdot f_1 + (v_{pz}^2(v_{pn}^2 - v_{px}^2) - v_{sz}^2(v_{pn}^2 \\ & + v_{pz}^2))f_1 \cdot f_2,\end{aligned}\tag{A-2}$$

where

$$\begin{aligned}f_1 &= k_x^2 \sin^2 \theta \cos^2 \phi + k_y^2 \sin^2 \theta \sin^2 \phi + k_z^2 \cos^2 \theta \\ &+ k_x k_y \sin^2 \theta \sin 2\phi + k_y k_z \sin 2\theta \sin \phi \\ &+ k_x k_z \sin 2\theta \cos \phi \\ f_2 &= k_x^2 + k_y^2 + k_z^2 - f_1.\end{aligned}\tag{A-3}$$

If we apply an inverse Fourier transform to these equations (using the relationships $k_x \leftrightarrow -i \frac{\partial}{\partial x}$; $k_y \leftrightarrow -i \frac{\partial}{\partial y}$; $k_z \leftrightarrow -i \frac{\partial}{\partial z}$; $\omega \leftrightarrow i \frac{\partial}{\partial t}$), we obtain the differential operators:

$$\begin{aligned}H_1 &= \sin^2 \theta \cos^2 \phi \frac{\partial^2}{\partial x^2} + \sin^2 \theta \sin^2 \phi \frac{\partial^2}{\partial y^2} + \cos^2 \theta \frac{\partial^2}{\partial z^2} \\ &+ \sin^2 \theta \sin 2\phi \frac{\partial^2}{\partial x \partial y} + \sin 2\theta \sin \phi \frac{\partial^2}{\partial y \partial z} \\ &+ \sin 2\theta \cos \phi \frac{\partial^2}{\partial x \partial z} \\ H_2 &= \frac{\partial^2}{\partial x^2} + \frac{\partial^2}{\partial y^2} + \frac{\partial^2}{\partial z^2} - H_1.\end{aligned}\tag{A-4}$$

Multiplying both sides of the dispersion relation (equation A-2) with the wavefield $p(\omega, k_x, k_y, k_z)$ considered to be the pressure wavefield and introducing the new auxiliary function (parameterized by a nonzero scalar α):

$$q(\omega, k_x, k_y, k_z) = \frac{(v_{pn}^2 - v_{sz}^2)f_2}{\alpha(\omega^2 - v_{sz}^2 f_2 - v_{pz}^2 f_1)} p(\omega, k_x, k_y, k_z),\tag{A-5}$$

equation A-2 can be written as

$$\begin{aligned}\omega^2 p(\omega, k_x, k_y, k_z) &= v_{px}^2 f_2 p(\omega, k_x, k_y, k_z) + v_{sz}^2 f_1 p(\omega, k_x, k_y, k_z) \\ &+ \alpha(v_{pz}^2 - v_{sz}^2) f_1 q(\omega, k_x, k_y, k_z).\end{aligned}\tag{A-6}$$

Applying an inverse Fourier transform to both sides of the previous two equations and using the relationships $k_x \leftrightarrow -i \frac{\partial}{\partial x}$; $k_y \leftrightarrow -i \frac{\partial}{\partial y}$; $k_z \leftrightarrow -i \frac{\partial}{\partial z}$; $\omega \leftrightarrow i \frac{\partial}{\partial t}$, the final equations can be written as

$$\begin{aligned}\frac{\partial^2 p}{\partial t^2} &= v_{px}^2 H_2 p + \alpha v_{pz}^2 H_1 q + v_{sz}^2 H_1 (p - \alpha q) \\ \frac{\partial^2 q}{\partial t^2} &= \frac{1}{\alpha} v_{pn}^2 H_2 p + v_{pz}^2 H_1 q - v_{sz}^2 H_2 \left(\frac{1}{\alpha} p - q \right).\end{aligned}\tag{A-7}$$

For seismic forward modeling, we must inject the source function in the right side of both equations.

REFERENCES

- Alkhalifah, T., 1998, Acoustic approximations for processing in transversely isotropic media: *Geophysics*, **63**, 623–631.
Alkhalifah, T., 2000, An acoustic wave equation for anisotropic media: *Geo-*

- physics, **65**, 1239–1250.
- Baysal, E., D. D. Kosloff, and J. W. C. Sherwood, 1983, Reverse time migration: *Geophysics*, **48**, 1514–1524.
- Du, X., R. Fletcher, and P. J. Fowler, 2008, A new pseudo-acoustic wave equation for VTI media: 70th Annual Conference and Exhibition, EAGE, Extended Abstracts, H033.
- Duveneck, E., P. Milcik, P. M. Bakker, and C. Perkins, 2008, Acoustic VTI wave equations and their application for anisotropic reverse-time migration: 78th Annual International Meeting, SEG, Expanded Abstracts, 2186–2190.
- Fei, T., J. A. Dellinger, G. E. Murphy, J. L. Hensley, and S. H. Gray, 1998, Anisotropic true-amplitude migration: 68th Annual International Meeting, SEG, Expanded Abstracts, 1677–1679.
- Fletcher, R., X. Du, and P. J. Fowler, 2008, A new pseudo-acoustic wave equation for TI media: 78th Annual International Meeting, SEG, Expanded Abstracts, 2082–2086.
- Fowler, P. J., X. Du, and R. Fletcher, 2008, Coupled equations for VTI modeling and migration: Presented at the 13th International Workshop on Seismic Anisotropy.
- Grechka, V., L. Zhang, and J. W. Rector, 2004, Shear waves in acoustic anisotropic media: *Geophysics*, **69**, 576–582.
- Hestholm, S., 2007, Acoustic VTI modeling using high-order finite-differences: 77th Annual International Meeting, SEG, Expanded Abstracts, 139–143.
- Klie, H., and W. Toro, 2001, A new acoustic wave equation for modeling in anisotropic media: 71st Annual International Meeting, SEG, Expanded Abstracts, 1171–1174.
- McMechan, G. A., 1983, Migration by extrapolation of time-dependent boundary values: *Geophysical Prospecting*, **31**, 413–420.
- Thomsen, L., 1986, Weak elastic anisotropy: *Geophysics*, **51**, 1954–1996.
- Tsvankin, I., 2001, *Seismic signatures and analysis of reflection data in anisotropic media*: Elsevier.
- Whitmore, N. D., 1983, Iterative depth migration by backward time propagation: 53rd Annual International Meeting, SEG, Expanded Abstracts, 827–830.
- Yan, J., and P. Sava, 2008, Elastic wavefield separation for VTI media: 78th Annual International Meeting, SEG, Expanded Abstracts, 2191–2195.
- Zhang, H., and Y. Zhang, 2008, Reverse time migration in 3D heterogeneous TTI media: 78th Annual International Meeting, SEG, Expanded Abstracts, 2196–2200.
- Zhou, H., G. Zhang, and R. Bloor, 2006a, An anisotropic acoustic wave equation for VTI media: 68th Annual Conference and Exhibition, EAGE, Extended Abstracts, H033.
- Zhou, H., G. Zhang, and R. Bloor, 2006b, An anisotropic acoustic wave equation for modeling and migration in 2D TTI media: 76th Annual International Meeting, SEG, Expanded Abstracts, 194–198.